

Improving Heat Transfer Performance in Two-pass Ribbed Channel by the Optimized Secondary Flow via Bend Shape Modification

Tieyu Gao¹, Jiangnan Zhu², Jun Li¹, Jianying Gong¹, Qingfeng Xia^{3,*}

1. Institute of Turbomachinery, School of Energy & Power Engineering, Xi'an Jiaotong University Xi'an, 710049, Shaanxi, China

2. Basic and Applied Research Center, Aero Engine Academy of China, No.21 Shunxing Road, Beijing, China

3*. Oxford Thermofluids Institute, Department of Engineering Science, the University of Oxford, Parks Road, Oxford OX1 3PJ, United Kingdom

Email: qingfeng.xia@eng.ox.ac.uk

Abstract: The heat transfer performance and friction loss of two-pass ribbed channels are highly influenced by the combined effect of rib orientation and bend shape. This paper, for the first time, numerically investigates this effect for four rib orientations, two rib angles and eight different bend shapes at Reynolds number of 30000. The results show that rib orientation determines the rotation direction and the transverse position of secondary flow in straight passages, while bend shape determines the delivery of upstream secondary flow and the generation of local secondary flow. The key to heat transfer enhancement in the second passage is to promote local secondary flow using energy from upstream secondary flow with the same rotation direction. The upstream secondary flow with the same rotation direction should be guided to a proper position, in order to enhance the dominant secondary flow in the second passage and reduce energy loss due to the undesirable secondary flow interaction. The impact of different bend shape on the secondary flow has been summarized. The round inner corner for the bend is preferred for the significant friction loss reduction and the excellent secondary flow energy delivery capacity. Meanwhile, the secondary flow generated by the square outer corner can significantly enhance the cooling performance at the entrance of the second passage for some certain rib orientations. An optimized combination of 60-degree rib orientation and bend shape can either thermal performance factor by 10 % in the second passage or reduce the friction loss by 22.3 % in the whole channel, compared with the existing experimental design. By contrast, it is found cooling performance and pressure loss are not sensitive to bend shape for the rib angel of 45-degree. The optimized bend shape is inspired by an intuitive visualization of secondary flow evolution, which provides insight on the geometry optimization for heat and mass transfer applications.

Keywords: Gas Turbine; Blade Cooling; Secondary Flow; Rib orientation; Bend Shape;

1. Introduction

Gas turbine has been widely used in aeronautical, marine propulsion and many other areas like electric power generation. Driven by the increasing fuel cost and the requirement of reducing CO₂ emission, the thermal efficiency of gas turbine has been continuously improved. The primary approach for the increased thermal efficiency is to raise turbine inlet temperature and pressure ratio. However, since the inlet gas temperature has already surpassed the melting point of metal components, the blades must be cooled to an allowable temperature for the specific metal material. Besides thermal barrier and film cooling on metal surfaces, internal

cooling is widely used in both vane and blade [1]. A typical internal cooling passage consists of several straight ribbed rectangular channels connected by 180-degree U-shaped bends. The cooling air from the compressor brings heat away from the internal cooling channel to cool the metal material. To enhance the heat transfer strength, ribs or other flow disturbing units are added to the channel surface at the cost of additional pressure loss. As a result, enhancing the heat transfer with the least pressure loss is the ultimate aim of the design of cooling channels.

In order to improve the cooling efficiency, a large amount of research of blade cooling has been conducted. Chandra and Han [2] experimentally investigate the heat transfer and friction performance of U-shaped channels with 45, 60, 90 degree ribs. The following investigation by Han and Zhang [3] indicates that the combined effect of rib orientation, rib angle and 180-degree sharp turn has strong an influence on the heat transfer and friction loss performance in downstream channel. The channel aspect ratio is another key geometrical parameter affecting the thermal performance in the ribbed channel. Siddique et al.[4, 5] numerically investigate the flow and heat transfer characteristics of an U-shaped smooth channel and a channel with 45-degree ribs. The results show the combined effect of variation of channel aspect ratio and bend has significant influence on local heat transfer.

The optimal rib angle and orientations have been intensively investigated, and the cross orientation with 45 degree or 60 degree ribs are preferred for better thermal performance. Al-Hadhrani et al. [6] investigate the effect of orientation of 45-degree ribs on heat transfer in two-pass channel, however, the results show that the parallel ribs have better heat transfer enhancement ability than the crossed ribs. Zhao and Tao [7] study 45 and 60 degree ribs in a two-pass cooling channel, and it is found rib angle orientation has a significant impact on convective mass transfer in the second passage. Moreover, the experimental work by Mochizuki et al.[8] presents both heat transfer performance and friction characteristics of 30, 45, 60, 75 and 90 degree ribs in U-shaped channel. The highest thermal performance is achieved by 60-degree rib cases; the performance is similar in the first passage but different in the bend region and the second pass due to the distinct rib orientation. The distinct thermal performance in the downstream pass is confirmed by the numerical work by Jang et al.[9].

Moreover, the heat transfer at the bend region and the second pass are highly influenced by the bend shape. Chyu [10] investigates the regional heat transfer performance in smooth two-pass and three-pass channels by analogous naphthalene mass transfer technique, indicating that the heat transfer enhancement due to the single turn in two-pass channel is 45-65% higher than that of the fully-developed region in the straight channel. However, this positive effect will be reduced when Reynolds number increases. The investigation of bend shape on overall heat transfer performance [11] suggests the symmetrical bulb (bend) configuration enhances the thermal performance factor by 41%. However, Erelli et al. [12] study the impact of bend geometry on flow and heat transfer characteristics of a smooth U-shaped channel, indicating that better heat transfer performance is obtained when the outer wall of the bend is sharply connected without round edge and the inner wall of the bend is hemi-circular shape. A recent numerical study of secondary flow in a two-pass channel with 45 degree ribs [13] shows that the secondary flow in the second passage is strongly influenced by the upstream secondary flow generated in the bend region and the first passage.

The work initiated by Han and Zhang[3] has suggested the significance of the combined effect of rib orientation, rib angle and bend shape on heat transfer and flow field in a U-shaped

channel. Furthermore, the experimental work by Mochizuki et al.[8] brings the pressure loss into the spotlight; the design of flow turbulators like ribs in cooling channel should enhance the heat transfer with the least pressure loss. The pressure loss can be reduced by the optimal secondary flow structure in the bend region and the downstream passage. However, existing studies focus either rib orientation or bend shape in multi-pass channel, a systematic investigation is not found for the combined effect of rib orientation and bend shape on flow field and heat transfer enhancement in the bend and the second passage.

Therefore, this numerical study investigates the combination of four rib orientations and eight kinds of bend shapes on the heat transfer and flow characteristics in U-shaped channels with 60-degree and 45-degree ribs. Based on the advanced vortex core visualization technology, the flow field especially the secondary flow structure is illustrated and its evolution is analyzed, which contributes to the understanding of heat transfer enhancement and friction reduction in a two-pass ribbed channel. A significant improvement in thermal performance and friction reduction is demonstrated with the modified bend geometry. Furthermore, design guidelines for the bend shape are proposed, taking the rib orientation and rib angle into account.

2. Computational method

2.1 Physical model

The geometry in this numerical study is based on the experiment model by Mochizuki et al.[8]. The channel width and height are both 44 mm and the length of this two-pass channel is 440 mm. A symmetric plane boundary condition is employed to reduce the mesh scale in the calculation, and thus only half of the channel height is shown in Fig.1 (a). Some of the squared corners of the bend in the existing experimental design are modified into round corners; eight bend shapes are investigated, shown in Fig. 1(b). The inner (I) and outer (O) bend wall has two different shapes: round (R) or square (S); the radius of the inner round bend (I) is 22 mm. The outer wall has round (R) or square (S) shape at two corners: left (L) and right(R); the radius of the outer round corner is 44 mm, maintaining the constancy of the channel width. The name of bend shape consists of two parts: the outer bend wall shape and the inner bend wall shape. For example, the bend which is named as OLRIS means that the left outer corner bend wall is round and the inner bend wall is square. Furthermore, four rib orientations in Fig.1 (d) are combined with those different bend shapes, in order to explore the optimized bend geometry. The rib height is 4 mm and the rib space is 44 mm. Identical with the experimental model, a space of 1 mm is set between rib end and side wall. In addition, the results are compared for two rib angles of 60 and 45 degree, which are the optimal angles suggested in an experimental study [14].

2.2 Mesh and boundary condition

The unstructured mesh consists of tetrahedral elements and prisms inflated from the wall boundary, see Fig 2(a). The near wall region has 20 inflation layers with a growth ratio of 1.2; the details of mesh are shown in Fig 2(b). The Y^+ value is guaranteed below 1. A mesh independence check has been performed using SST turbulence model for the case of 60NP OSIS, on meshes with about 1, 2, 3, 6, 9, 11 and 14 million. The mesh independence has been achieved when the node number is larger than 9.27 million, see Fig. 2(c), according to the convergence of local Nusselt number ratio on the centerline of ribbed wall between the No.2 and No.3 ribs of Passage 1. Therefore, the mesh with 9.27 million node and 20 inflation layers is adopted in this study.

This numerical study is conducted by the commercial software ANSYS CFX 14.0 with the Shear Stress Turbulence (SST) turbulence model, which has been proved to have satisfying accuracy in the simulation of ribbed channel [15-17]. In this numerical study, boundary conditions are selected to mimic the experimental work of Mochizuki et al. [8]. The symmetric condition is set at the symmetrical plane. The inlet pressure of channel is 1 atm and the air inlet temperature is 298 K using ideal gas model. The inlet turbulent intensity is set as 5% and the mass flow rate is used at the outlet plane to maintain the inlet Reynolds number at 30000. The no-slip wall condition and a constant temperature of 338 K are set for wall. Notably, the appropriation of the constant temperature wall boundary is justified in a recent numerical study [19]. The flow in the near wall region is treated by the automatic wall function in CFX. The convergence criterion is set as 10^{-5} for the Root Mean Square (RMS) error.

2.3 Data reduction

The Reynolds number is computed by

$$Re = \frac{\rho V D_h}{\mu} \quad (1)$$

where D_h is the hydraulic diameter of the passage; V is area-averaged velocity in the channel inlet plane; μ is the dynamic viscosity of air; ρ is air density.

The local Nusselt number Nu is calculated by Eq. (2) where k is the thermal conductivity of the flow. The local heat transfer coefficient h is defined in Eq. (3). The parameter q is the wall heat flux; T_w is wall temperature and bulk flow temperature T_b is calculated by interpolating the outlet and the inlet temperatures, assuming a linear steam temperature rise along the flow channel.

The baseline Nusselt number Nu_0 is defined in Eq. (4), as the fully-developed turbulent nonrotating straight smooth tube flow, where the value of Pr is fixed as 0.71 for air.

$$Nu = \frac{h D_h}{k} \quad (2)$$

$$h = \frac{q}{T_w - T_b} \quad (3)$$

$$Nu_0 = 0.023 Re^{0.8} Pr^{0.4} \quad (4)$$

In order to simplify the post-processing of Nusselt number contour, $T_w - T_b$ is calculated by the logarithmic mean temperature difference defined by Eq. (5), where T_{out} and T_{in} are the outlet and inlet temperature of the control volume, respectively.

$$\Delta t_m = \frac{T_{out} - T_{in}}{\ln \frac{T_w - T_{in}}{T_w - T_{out}}} \quad (5)$$

According to the experimental work by Mochizuki et al.[8], the friction factor f is defined as:

$$f = 2 \Delta p (D_h / L) / (\rho V^2) \quad (6)$$

where Δp is the pressure drop through the whole passage and L is the distance from the inlet to the outlet along the centerline of the passage.

In addition, a non-dimensional thermal performance factor TF is defined in this study, as a balance of pressure loss and heat transfer enhancement in a ribbed channel:

$$TF = \frac{Nu/Nu_0}{(f/f_0)^{1/3}} \quad (7)$$

where the baseline of friction factor f_0 is defined as that of straight smooth channel:

$$f_0 = (1.58 \ln Re - 3.28)^{-2} \quad (8)$$

Since secondary flow is the key to enhanced cooling in the ribbed channel, the vortex core visualization technology that illustrates the shape and distribution of vortex are applied to display the interaction and evolution of secondary flows intuitively. There are several definitions for vortex core, while λ_2 method is found more appropriate in ribbed channel study [18,19]. This method is based on the anti-symmetric components of velocity gradient tensor

$S = \frac{D+D^T}{2}$ and the symmetric components of velocity gradient tensor $\Omega = \frac{D-D^T}{2}$, where D is the velocity gradient tensor.

$$D = [d_{ij}] = \begin{bmatrix} \frac{\partial u}{\partial x} & \frac{\partial u}{\partial y} & \frac{\partial u}{\partial z} \\ \frac{\partial v}{\partial x} & \frac{\partial v}{\partial y} & \frac{\partial v}{\partial z} \\ \frac{\partial w}{\partial x} & \frac{\partial w}{\partial y} & \frac{\partial w}{\partial z} \end{bmatrix} \quad (9)$$

λ_2 is the second largest real eigenvalues of the tensor $S^2 + \Omega^2$, and the region with $\lambda_2 < 0$ is the vortex core.

3. Results and Discussion

3.1 Validation of the Numerical Method

The numerical results of regional-averaged Nusselt number ratio for 60 NN OSIS, 60 NP OSIS, 60 PN OSIS and 60 PP OSIS cases are validated by the experimental data of Mochizuki et al.[8], shown in Fig.3 (a). The ribbed wall of this U-shaped channel is divided into three parts: Passage 1 (P1) ribbed wall, Passage 2 (P2) ribbed wall and bend wall. The outlet of Passage 1 and the inlet of Passage 2 have the same coordination with the inner corner wall. The numerical results agree with the experimental data in trend with minor discretion. The largest relative error is about 9.4% for the 60 PP OSIS case. In addition, the friction factors of these four cases agree with the experimental data, shown in Fig.3 (b). The comparison of heat transfer performance and friction factor between numerical results and experimental data suggests that this numerical model is capable of predicting the heat transfer performance and flow characteristics in this two-pass ribbed channel.

3.2 Heat transfer performance

The regional-averaged Nusselt number ratio and friction factor for cases with 60 degree rib angle and different rib orientations are shown in Figs. 4. First of all, it can be seen that the

averaged Nusselt number ratio in Passage 1 is not significantly influenced by the bend shape and rib orientation. On the contrary, heat transfer performance in Passage 2 is strongly influenced by the combination effect of rib orientation and bends shape. Meanwhile, thermal the performance in the bend depends on the rib orientation in Passage 1 and the bend shape, but it is not sensitive to rib orientation in passage 2. Secondly, N-type rib orientation in Passage 1 leads to a better performance in the bend region and Passage 2, despite of bend shapes. The overall performance of PN and NP is similar, but a significant improvement in heat transfer in Passage 2 is found for the cases of 60 NP ORRIS and 60 NP OLRIR. Therefore, the NP rib orientation is the optimal for the two-pass channel.

The inner round wall can reduce the pressure loss without deteriorating the cooling performance significantly. The cases of ORRIR and OLRIR have a similar low pressure loss as the case of ORIR, lower than the baseline case of OSIS as in the experimental design. On the other hand, the outer round walls also reduce the pressure loss to some extent, but the square outer wall may generate the secondary flow structure enhancing the cooling in Passage 2 significantly. The heat transfer performance for the case of ORIR is lowest in the bend region. Thereby, the contribution of outer wall shape should be discussed together with the secondary flow evolution in Passage 2. For the group of 60 NP cases, the bend shape of outer right round wall and inner square wall (ORRIS) has the best cooling performance, while pressure loss is the highest. The thermal performance in the bend is positively correlated with the pressure loss for most cases. The bend shape of outer right round wall and round inner wall (OLRIR) has a similar thermal performance with the baseline case (OSIS), i.e. bend with both inner and outer square wall as in the existing experimental study, but the pressure loss is significantly reduced by 9%.

For the group of 60 PN cases, the bend shape of outer right round wall and inner square wall (ORRIS) also has the best cooling performance. The thermal performance is similar in Passage 1 and lower in Passage 2, while pressure loss is apparently lower than the corresponding 60 NP case. Notably, the case of 60 PN OSIS, all square corners as in the experimental bend shape design, has the highest pressure loss, instead of 60 PN ORRIS. It suggests the thermal factor (TF) of this group can be comparable with that of 60 NP, considering both heat transfer gain and pressure loss. The groups of 60 NN and 60 PP cases are not favored for the worse thermal performance, compared with the cross rib orientation.

The thermal performance factor, as a compromise of cooling performance and pressure loss, is compared for different bend shapes, rib angles and rib orientations. Fig. 5 (a) shows the cross rib orientation leads to higher TF than the parallel ones, i.e. 60 NN and 60 PP. The group of 60 PN have the higher TF than the group of 60 NP, although the heat transfer performance is lower as in Figs. 4. In particularly, the highest TF is found for 60 PN OLRIR, while the case of 60 PN OSIS has the lowest TF due to the high pressure drop, see Fig. 4 (c). Thermal factors are not sensitive to rib orientation for 45 degree ribs as those with 60 degree ribs, and thus they are not shown in this paper. Similar with those of 60 degree, the round corner wall at the bend leads to higher TF, which leads to TF similar with that of 60 PN OLRIR but worse cooling performance.

The optimal bend shape should be chosen as a compromise of heat performance and thermal factor. The heat performance is quantified by the averaged Nu ratio of the whole channel wall, see Fig. 5 (b); the highest value of Nu ratio is obtained by the case 60 NP ORRIS,

but the highest TF is found for 60 PN OLRIS. For the similar cooling performance, the case of 60 PN OLRIR increases TF by 6% over the optimal experimental design of 60 NP OSIS, indicating a significant reduction in pressure loss. The baseline case of square bend shape (OSIS) has neither the highest Nu ratio nor the highest TF. The significant higher Nu ratio of the case 60 NP ORRIS should be chosen, with 2.0% increase in TF and 3.1% increase in Nu ratio over the baseline case of 60 NP OSIS. Meanwhile, the case of 60 PN OLRIR increases TF by 10%, compared with the baseline case of 60PN OSIS.

3.3 Influence of secondary flow on heat transfer and friction loss

Fig.6 shows the secondary flow in 60 NP cases with 8 different bend shapes. First of all, the ORRIS bend shape has the preferred secondary flow structure in Passage 2, leading to the highest cooling performance. The dominant secondary flow forms at the entrance and sweeps the whole width of Passage 2. Fig. 6 (a) and (b) show the P1 outer square corner, which does not generate useful secondary flow, should be replaced by a round fillet to reduce pressure loss. Although the round inner and outer wall (ORIR) result in the least pressure loss, the secondary flow along the main flow in Passage 2 is suppressed by the strong upstream secondary flow. The reason of suppression should be attributed to size, strength and position of upstream vortex core. Meanwhile, the square inner bend reduces the size of the P1 main flow secondary flow but contributes to the P2 Corner Generated Secondary flow which is crucial to enhance thermal performance in Passage 2. The P2 Main Flow Secondary Flow has the same rotating direction with the P2 Corner Secondary Flow, according to the secondary flow rotation in Fig. 7 (b). The P2 Corner Generated Secondary flow is guided by the first rib to the bottom of the inner wall and serves as the seed for the influencing secondary flow in Passage 2. The case ORRIS has a similar secondary flow structure with the case of OSIS in Passage 1 and the bend, but the P2 Main Flow Secondary Flow for ORRIS is bigger in size resulting in a better cooling performance.

Secondly, upstream secondary flow contributes to the local heat transfer, depending on its position and rotating direction. Inner round wall can deliver more upstream secondary flow energy to Passage 2. According to Fig. 6 (c), inner round bend has delivered two streams of secondary flow, which survive until the third rib in Passage 2. However, the P2 Main Flow Secondary Flow, the P1 Corner Secondary Flow in NP cases are all opposite to the P1 Main Flow Secondary Flow. For example, Fig. 6 (e) and (g) show that the strong P1 Main Flow Secondary Flow has a negative impact on the generation of the P2 Corner Generated Secondary Flow and the development of the P2 Main Flow Secondary Flow. Therefore, the P1 Main Flow Secondary Flow should be fully dissipated in the bend region which could not only enhance the heat transfer in the bend but also reduce the negative influence on heat transfer in Passage 2. For example, the thermal performance of 60 NP ORIS case is poor for the upstream secondary flow dwelling in the outer wall of Passage 2 entrance, which delays the formation of the P2 Main Flow Secondary Flow. However, the cases of 60 NP ORIR and OSIR have a reasonable thermal performance for strong but independent secondary flow streams in Passage 2.

Fig.7 shows velocity vectors on the channel cross-sections for several selected cases of the 60 NP group. The velocity component normal to the cross-section is not plotted, in order to illustrate only the secondary flow rotation. The A-E and B-D planes are 6.82 and 8.18 times D_h away from the inlet plane, respectively. The plane C is in the middle of the bend between Passage 1 and Passage 2. The rotation direction of the P1 and P2 Main Flow Secondary Flow

are opposite, determined only by the rib orientation. Fig.7 shows that the rotation direction of the P2 Main Flow Secondary Flow is clockwise viewing against main flow direction, opposite to the P1 Main Flow Secondary Flow but same with the Bend Generated Secondary Flow.

The case 60 NP ORRIS demonstrates the process of cooperative interactions between upstream secondary flow and local secondary flow in passage 2. On plane C of the case 60 NP ORRIS, it is shown that dominant Bend Generated Secondary Flow has an anti-clockwise rotation viewed against the main flow direction, and it is opposite to the upstream P1 Main Flow Secondary Flow. These secondary flow streams destroy each other at P2 entrance where the P2 Corner Generated Secondary Flow is the only dominant structure, demonstrated in the vector plot at the cross-section D (Fig.7 (b)). Furthermore, the P2 Corner Generated Secondary Flow has a clockwise rotation viewed against the main flow direction, contributing directly to the formation of the P2 Main Flow Secondary Flow.

The dominant secondary flow near P2 entrance is crucial for the secondary flow development in Passage 2, which could be the P1 or P2 Corner Generated Secondary Flow. It is shown in Fig.6 (c) and (e) that a strong P1 Corner Generated Secondary Flow lies at the bottom of the two split streams of the P1 Main Flow Secondary Flow, whose rotation directions are anti-clockwise viewing against the streamwise direction, shown in Plane C of Fig. 7 (a). According to the investigation by Xia et al. [20], two back-to-back vortices with the opposite rotation directions can stabilize each other; both streams of the P1 Main Flow Secondary Flow and the P1 Corner Generated Secondary Flow reach Passage 2 independently. Since the rib orientation is different in Passage 2, the P2 Main Flow Secondary Flow with the opposite rotation lies near the inner wall of Passage 2. Although inner round bend can deliver more energy from the P1 Main Flow Secondary Flow, but it cannot contribute directly into the formation of the P2 Main Flow Secondary Flow for the distinct rotating direction. At the same time, the P2 Corner Generated Secondary Flow can accelerate the formation of main flow secondary flow for the same rotation direction in spite of rib orientation, see the large size of secondary flow in Passage 2 in Fig. 7 (b) and Fig. 6 (f).

The contours of Nusselt number ratio distribution on ribbed wall are shown in Fig.8. Strong secondary flow results in high Nu region, especially for the P2 Corner Secondary Flow. For the channel with angled ribs, the separate-reattach process caused by angled ribs in near-wall region can suppress the growth of boundary layer and enhance the local turbulence strength, which directly raises the local heat transfer strength [18]. The Nu ratio on the bottom surface in Passage 1 is higher than that in Passage 2, it suggests the inter-rib secondary flow plays a more significant role in Passage 1. High Nu regions can be observed on the outer side wall in Passage 1, where inter-rib secondary flow crushes. The inter-rib secondary flow also offers rotation velocity to the main flow secondary flow in ribbed passages. On the other hand, the larger size of the main flow secondary flow sweeping side wall contributes to heat transfer on bottom and side walls. The P1 and P2 Main Flow Secondary Flow could largely enhance the mass transfer between near wall region and main flow region and thus enhances the temperature difference in heat convection, which is also an important factor for heat transfer enhancement. Therefore, the integral Nu ratio in Passage 2 has a similar value as in Passage 1, see Fig. 4 (b).

Fig.9 shows the secondary flow evolution for 60 PN cases, and Fig. 10 shows velocity vectors on selected cross-sections for OSIS, ORRIR and OLRIR cases of the 60 PN group. It is shown that the P1 Main Flow Secondary Flow stays near the inner wall of P1 while the P2

Main Flow Secondary Flow is near the outer wall of Passage 2. However, P1 Main Flow Secondary Flow is not delivered into the bend and Passage 2, since the bend suppresses the secondary flow generated by the P-type rib orientation in Passage 1. It is confirmed in velocity plot in Fig. 10. The P1 Corner Generated Secondary Flow is generated by the combination of the square right outer corner and the round inner corner. Similarly, the Bend Generated Secondary Flow is only generated by the square inner corner. At the same time, the strong P2 Corner Generated Secondary Flow generated by the square outer corner in Passage 2 does not contribute to the formation of P2 Main Flow Secondary Flow sufficiently as in NP case, due to the distinct rotating direction and position. In passage 2, the development of the secondary flow is not affected by P1 Main Flow Secondary Flow, but adversely impacted by the P2 Corner Generated Secondary Flow.

Fig.10 (a) shows that the dominant P1 Corner Generated Secondary Flow has the opposite rotation direction to the upstream secondary flow on Plane C, suggesting that the P1 Main Flow Secondary Flow can not pass through the bend. As a result, the P1 Main Flow Secondary Flow fails to flow into Passage 2, leading to a stronger P1 Corner Generated Secondary Flow than that of NN and NP cases. The strength of the P1 Corner Generated Secondary Flow can be shown by the size of the vortex core method in Fig. 9. Secondly, the weaker P1 Corner Generated Secondary Flow due to the round outer corner, shown on Plane C of Fig.10 (b), is a strong evidence for the promotional effect of the square right outer corner. The square inner corner generates a stream secondary flow which has the same rotating direction with the stronger P1 Corner Generated Secondary Flow, see Plane C of Fig.10 (c).

On the other hand, the strength of the P2 Corner Generated Secondary Flow depends on the outer left corner shape and the strength of the P1 Corner Generated Secondary Flow. P1 and P2 Corner Generated Secondary Flow have the same rotating direction, but the fully developed P1 Corner Generated Secondary Flow has a negative impact on the generation of the P2 Corner Generated Secondary Flow, suggested by Fig. 9 (a) and (g). The square inner bend reduced the strength of the P1 Corner Generated Secondary Flow, and thus the P2 Corner Generated Secondary Flow is less impacted for the case of OSIS, see Fig. 9 (h). In other words, it is the square outer right corner that has a negative impact on the P2 Corner Generated Secondary Flow. Meanwhile, the square outer left corner has an evident promotion on the P2 Corner Generated Secondary Flow. Without the suppression of the P1 Main Flow Secondary flow, the strength of the P2 Corner Generated Secondary Flow is stronger than that in the NP group.

Furthermore, the existence of P2 Corner Generated Secondary Flow also brings in additional friction loss for the PN rib orientation. P1 and P2 Corner Generated Secondary Flow have the different impact on pressure loss and cooling performance. The cases without the P2 Corner Generated Secondary Flow such as OLRIR and OLRIS cases show better heat transfer and friction loss performance, indicating that the existence of P1 Corner Generated Secondary Flow and the Bend Generated Secondary Flow has better ability on heat transfer enhancement than the P2 Corner Generated Secondary Flow.

The P2 Corner Generated Secondary Flow has the distinct rotating direction depends on the rib orientation in Passage 2, while its rotation direction is same with the P2 Main Flow Secondary Flow for both NP and PN groups. Because of the identical rotation direction, it is desirable to fully utilize the P2 Corner Generated Secondary Flow's energy to enhance the P2 Main Flow Secondary Flow development, in order to enhance the heat transfer performance in

Passage 2. However, for the PN cases, the P2 Corner Generated Secondary Flow is directed to the inner wall of Passage 2, while the P2 Main Flow Secondary Flow forms at the outer side wall in Passage 2. In contrast to the promotional effect on the P2 Main Flow Secondary Flow for NP cases, there is no sign of the P2 Main Flow Secondary Flow promotion in Passage 2 for PN cases, according to the vortex core visualization in Fig. 9. Judging from the velocity on Plane D of Fig. 10 (c), the P2 Corner Generated Secondary Flow suppresses the inter-rib vortex, due to the flow velocity collision near the rib top. As a result of collision, the rotating energy of ribs secondary flow can not merge with the P2 Main Flow Secondary Flow and excessive flow loss is found for the case of 60 PN OSIS, see Fig. 4 (c). Nevertheless, the existence of the P2 Corner Generated Secondary Flow may generate a small stream of P2 Corner Generated Secondary Flow between the larger stream of P2 Corner Generated Secondary Flow and the outer side wall of Passage 2 (Fig. 10 (b-c)), which is anti-clockwise direction. This small stream of P2 Corner Generated Secondary Flow locates just above the rib top which is also the position of the P2 Main Flow Secondary Flow formation. This secondary flow has a negative influence on secondary flow between ribs and the P2 Main Flow Secondary Flow for PN cases. By comparing between 60 PN OSIR and OSIS cases, it can be seen that the P2 Corner Generated Secondary Flow is weakened in OSIR case and leads to higher Nusselt number ratios in Passage 2 and lower friction loss than those of OSIS case.

The shape and rotation direction of secondary flows in Passage 1 and the corner are nearly the same for PP and NN cases with the same bend shape, but the cooling performance in Passage 2 is less than that of cross rib orientation, i.e. NP and PN cases [18]. The rib angle of 45 degree leads to similar but weaker secondary flow as the corresponding cases with 60 degree ribs. Therefore, only representative cases are illustrated in this paper.

3.5 Bend shape effect on heat transfer and friction loss

Table 1 Summary of bend shape effect on secondary flow evolution

Position	Type	P1 Corner Generated Secondary Flow	Bend Generated Secondary Flow	P2 Corner Generated Secondary Flow
Outer R P1	Square	Strong Promotion	Not affected	Slight Suppression
	Round	Strong Suppression		Promotion
Inner	Square	Suppression	Generated	Promotion
	Round	Promotion	Not Generated	Suppression
Outer L P2	Square	Slight Suppression	Not affected	Strong Promotion
	Round	Slight Promotion		Suppression

According to vortex core visualization method, the contribution of different bend shapes to secondary flow development near the bend is summarized in Table 1. It can be observed that the outer corners directly affect the local corner generated secondary flow and slightly influence the secondary flow generated by the other outer corners. The shape of the inner corner wall only determines the generation of bend generated secondary flow, but has a significant impact on the upstream secondary flow delivery. The square inner wall has a positive effect on the corner generated secondary flow while the round one has a negative impact. The suppressed P1 Corner Generated Secondary Flow is favored for the growth of P2 Corner Generated Secondary Flow. According to this table, certain secondary flow can be enhanced or suppressed by a modified bend shape. By direct control of secondary flow via bend shape and rib orientation, it is possible to optimize the secondary flow in a two-pass ribbed channel, in order to enhance the

heat transfer and friction loss performance.

4. Conclusion

The combined effect of rib-orientation and bend shape on heat transfer and friction loss in U-shaped channel with 60 degree and 45 degree ribs is numerically investigated and analyzed by vortex core technology. Several conclusions are obtained below:

Firstly, the key point of flow management in U-shaped channel is to enhance the growth of the P2 Main Flow Secondary Flow as possible using upstream secondary flow and reduce the interaction between nearby secondary flows. The upstream secondary flow with the same rotation direction at the same position of the P2 Main Flow Secondary Flow could directly and largely enhance the development of the P2 Main Flow Secondary Flow, which enhances the heat transfer and reduces energy loss in Passage 2.

Secondly, for NP cases, since the P1 Main Flow Secondary Flow can be redirected into Passage 2 with an opposite rotation direction to the P2 Main Flow Secondary Flow, P1 Main Flow Secondary Flow should dissipate near the P2 inlet region to avoid its negative effect on the local secondary flow in Passage 2. The bend shape should generate the preferred P2 Corner Generated Secondary Flow, which could directly enhance the P2 Main Flow Secondary Flow. For PN cases, since the P1 Main Flow Secondary Flow is difficult to enter Passage 2, the P1/P2 Corner Generated Secondary Flow and the Bend Generated Secondary Flow are the key factors in Passage 2. Because the strong P2 Corner Generated Secondary Flow has a negative effect on Secondary Flow between Ribs and the P2 Main Flow Secondary Flow, round R-corner and inner corner wall are preferred for the reduced friction loss.

Thirdly, the impact of the bend shape on the downstream secondary flow is summarized. The round inner wall prevents the generation of the Bend Generated Secondary Flow; it can largely reduce the energy loss due to secondary flow interaction and the energy dissipation of the P1 Main Flow Secondary Flow in the bend. Meanwhile, the shape of outer corner wall of the bend can directly determine the formation of local corner secondary flow and slightly influence the upstream or downstream secondary flow. The square outer corner generates P1/P2 Corner Generated Secondary Flow, which have positive effect on the heat transfer in Passage 2 with certain rib orientation. By optimizing the rib orientation and bend shape, it is possible to enhance the heat convection by control the certain secondary flow, e.g., the case 60 NP ORRIS should be chosen, with 2.0% increase in TF and 3.1% increase in Nu ratio than the baseline case of 60 NP.

Finally, the intuitive visualization of secondary flow evolution provides hints for geometry optimization. In addition to a parameter study (varying length scale for some selected geometrical parameters), introducing new geometric feature is promising to enhance heat and mass transfer in flow. Geometry modification based on secondary flow visualization, as elaborated in this paper, provides a new tool for flow control and design optimization.

Acknowledgement

This work supported by Research Program supported by the [National Natural Science Foundation of China] under Grant [No.50806059]; the [Innovative Research Team in University of Ministry of Education of China] under Grant [IRT1280].

References

- [1] J.C. Han, S. Dutta, S. Ekkad, Gas Turbine Heat Transfer and Cooling Technology, Second Edition. Second Edition ed., CRC Press 2012.
- [2] P.R. Chandra, J.C. Han, Pressure drop and mass transfer in two-pass ribbed channels, *Journal of Thermophysics and Heat Transfer* 3 (1989) 315-320.
- [3] J.C. Han, P. Zhang, Effect of Rib-Angle Orientation on Local Mass Transfer Distribution in a Three-Pass Rib-Roughened Channel, *Journal of Turbomachinery* 113 (1991) 123-130.
- [4] W. Siddique, I.V. Shevchuk, L. El-Gabry, N.B. Hushmandi, T.H. Fransson, On flow structure, heat transfer and pressure drop in varying aspect ratio two-pass rectangular channel with ribs at 45°, *Heat and Mass Transfer* 49 (2013) 679-694.
- [5] W. Siddique, L. El-Gabry, I.V. Shevchuk, N.B. Hushmandi, T.H. Fransson, Flow Structure, Heat Transfer and Pressure Drop in Varying Aspect Ratio Two-Pass Rectangular Smooth Channels, *Heat and Mass Transfer* 48 (2012) 735-748.
- [6] L. Al-Hadhrami, J. Han, Effect of rotation on heat transfer in two-pass square channels with five different orientations of 45° angled rib turbulators, *International Journal of Heat and Mass Transfer* 46 (2003) 653-669.
- [7] Y.C. Zhao, Q.W. Tao, Effect of rib angle orientation on local mass transfer distribution around sharp 180 deg turn with rib-turbulators mounted in entire two-pass channels, *Heat and Mass Transfer* 32 (1997) 325-332.
- [8] S. Mochizuki, A. Murata, M. Fukunaga, Effects of rib arrangements on pressure drop and heat transfer in a rib-roughened channel with a sharp 180 deg turn, *Journal of Turbomachinery* 119 (1997) 610-616.
- [9] Y.J. Jang, H.C. Chen, J.C. Han, Computation of Flow and Heat Transfer in Two-pass Channels with 60 Deg Ribs, *Journal of Heat Transfer* 123 (2001) 563-575.
- [10] M.K. Chyu, Regional Heat Transfer and Pressure Drop in Two-Pass and Three-Pass Flow Passages with 180-Degree Sharp Turns, ASME International Gas Turbine & Aeroengine Congress & Exposition (1989).
- [11] K. Saha, S. Acharya, Effect of bend geometry on heat transfer and pressure drop in a two-pass coolant square channel for a turbine, *Journal of Turbomachinery* 135 (2012) 319-329.
- [12] R. Erelli, A.K. Saha, P.K. Panigrahi, Influence of turn geometry on turbulent fluid flow and heat transfer in a stationary two-pass square duct, *International Journal of Heat and Mass Transfer* 89 (2015) 667-684.
- [13] J. Zhu, T. Gao, J. Li, G. Li, J. Gong, Numerical Investigation of Secondary Flow Vortex Core Structure in the Two-pass Rectangular Channel with 45° Ribs., Montreal, Canada, 2015.
- [14] J.S. Park, J.C. Han, Y. Huang, S. Ou, R.J. Boyle, Heat transfer performance comparisons of five different rectangular channels with parallel angled ribs, *International Journal of Heat and Mass Transfer* 35 (1992) 2891-2903.
- [15] D. Walker, J. Zausner, RANS evaluations of internal cooling passage geometries: Ribbed passages and a 180 degree bend., Montreal, Canada, 2007, pp. 645-660.
- [16] F. Farisco, S. Rochhausen, M. Korkmaz, M. Schroll, Validation of flow field and heat transfer in a two-pass internal cooling channel using different turbulence models. 2013, pp. V3A-V12A.
- [17] M. Schuler, H.M. Dreher, S.O. Neumann, B. Weigand, M. Elfert, Numerical Predictions of the Effect of Rotation on Fluid Flow and Heat Transfer in an Engine-Similar Two-Pass Internal Cooling Channel with Smooth and Ribbed Walls, *Journal of Turbomachinery-Transactions of the ASME* 134 (2012) 21021.

- [18] Numerical study of conjugate heat transfer of steam and air in high aspect rectangular ribbed cooling channel, T. Gao, J. Zhu, C. Liu and J. Xu: Journal of Mechanical Science and Technology., 30(2016), 1431-1442.
- [19] T. Gao, J. Zhu, J. Li, Q. Xia, Numerical study of the influence of rib orientation on heat transfer enhancement in two-pass ribbed rectangular channel, Engineering Applications of Computational Fluid Mechanics (2017) 1-20.
- [20] Q. Xia, S. Zhong, Enhancement of laminar flow mixing using a pair of staggered lateral synthetic jets, Sensors and Actuators A: Physical 207 (2014) 75-83.

Figure Caption

Fig.1 Schematic of model;(a) Geometry of model (60 NP ORIR); (b) Bend shape; (c) Parameters of bend; (d) Rib orientation

Fig.2 Mesh independency check and mesh arrangement; (a) Mesh for the corner of two-pass channel; (b) Mesh on channel cross-section; (c) Mesh independence check

Fig.3 Numerical result validated by experimental data; (a) Regional-averaged Nusselt number ratio; (b) Friction factor

Fig.4 Heat transfer and friction loss characteristics in channel with 60-degree ribs and different corner shapes; (a) 60 NN cases; (b) 60 NP cases; (c) 60 PN cases; (d) 60 PP cases

Fig.5 Thermal performance of the overall channel (a) TF with 60-degree ribs; (b) Nusselt ratios

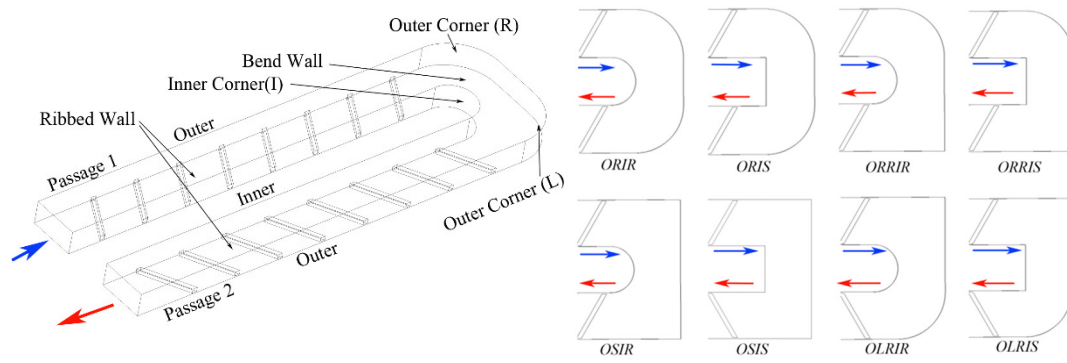
Fig.6 Secondary flow structure in 60 NP cases

Fig. 7 Rotation direction of secondary flow in NP cases; (a) 60 NP OLRIR; (b) 60 NP ORRIS; (c) 60 NP OSIS; (d) 60 NP ORIR

Fig.8 Nusselt number distribution contour; (a) NP channel; (b) PN channel

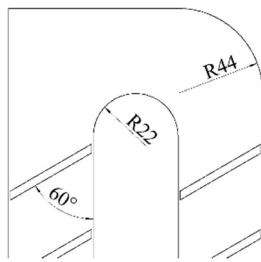
Fig.9 Secondary flow in PN cases

Fig. 10 Rotation direction of secondary flow in PN cases; (a) 60 PN OLRIR; (b) 60 PNORRIR; (c) 60 PN OSIS

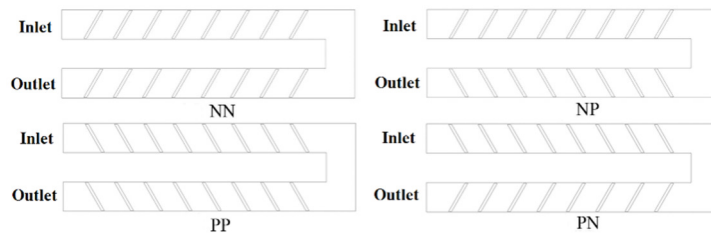


(a) Geometry of model (60 NP ORIR)

(b) Bend shape

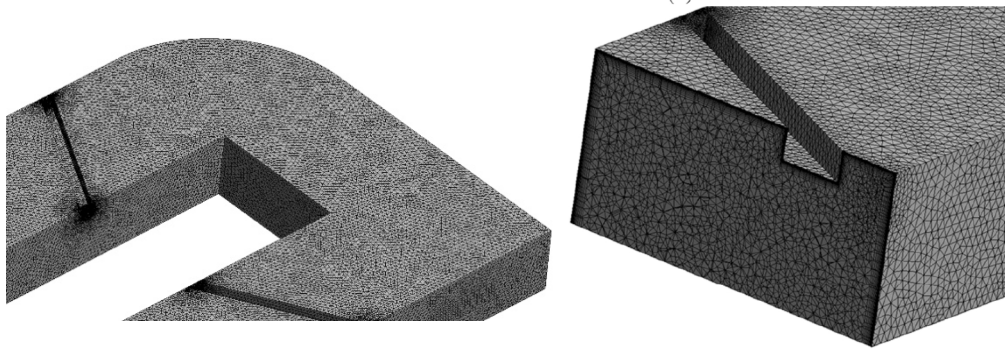


(c) Parameters of bend

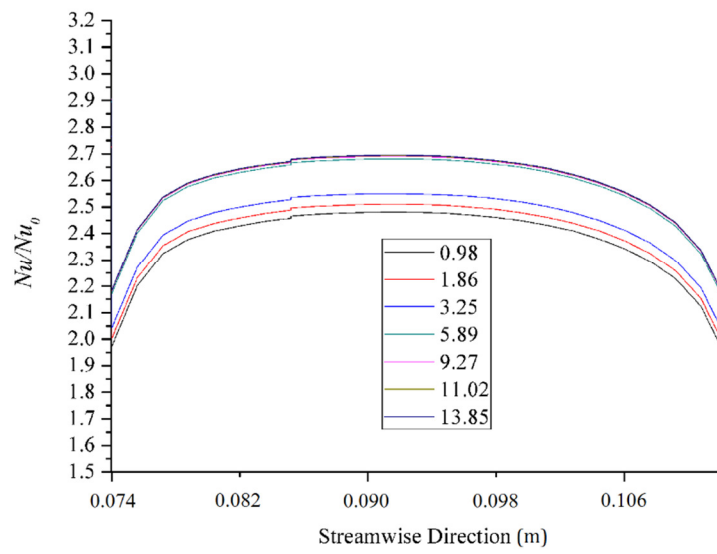


(d) Rib orientation

Fig.1 Schematic of model

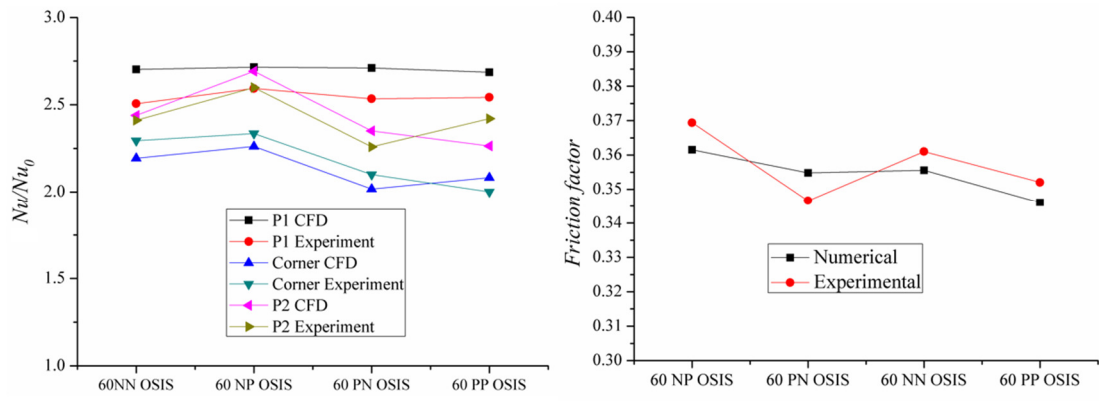


(a) Mesh for the corner of two-pass channel (b) Mesh on channel cross-section



(c) Mesh independence check

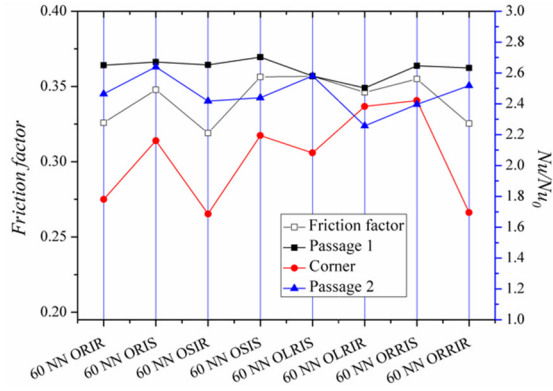
Fig.2 Mesh independency check and mesh arrangement



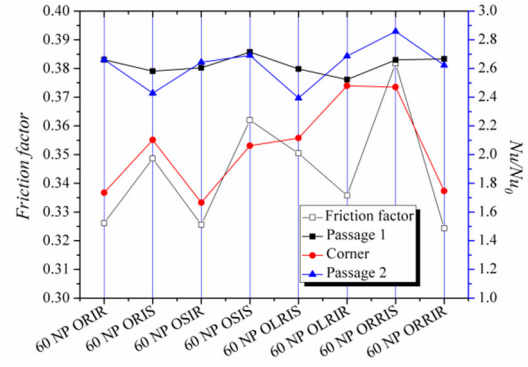
(a) Regional-averaged Nusselt number ratio

(b) Friction factor

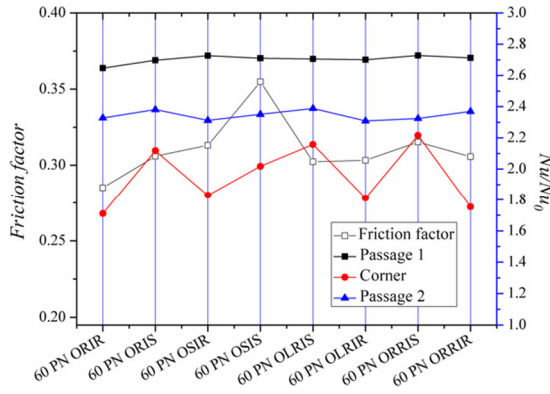
Fig.3 Numerical result validated by experimental data



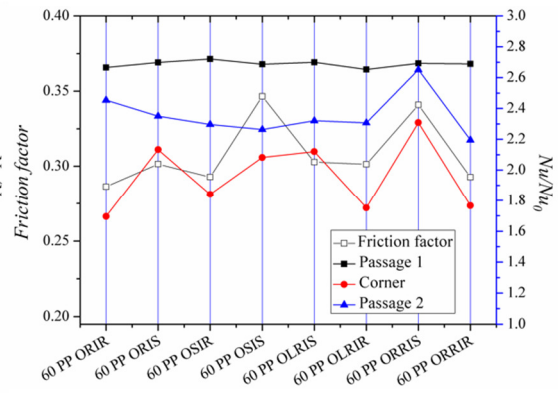
(a) 60 NN cases



(b) 60 NP cases

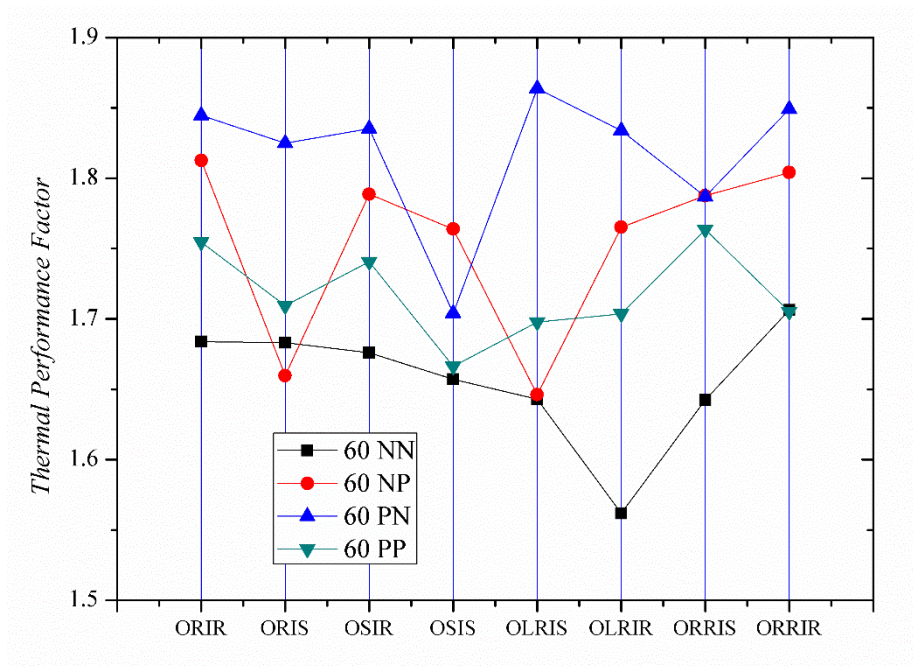


(c) 60 PN cases

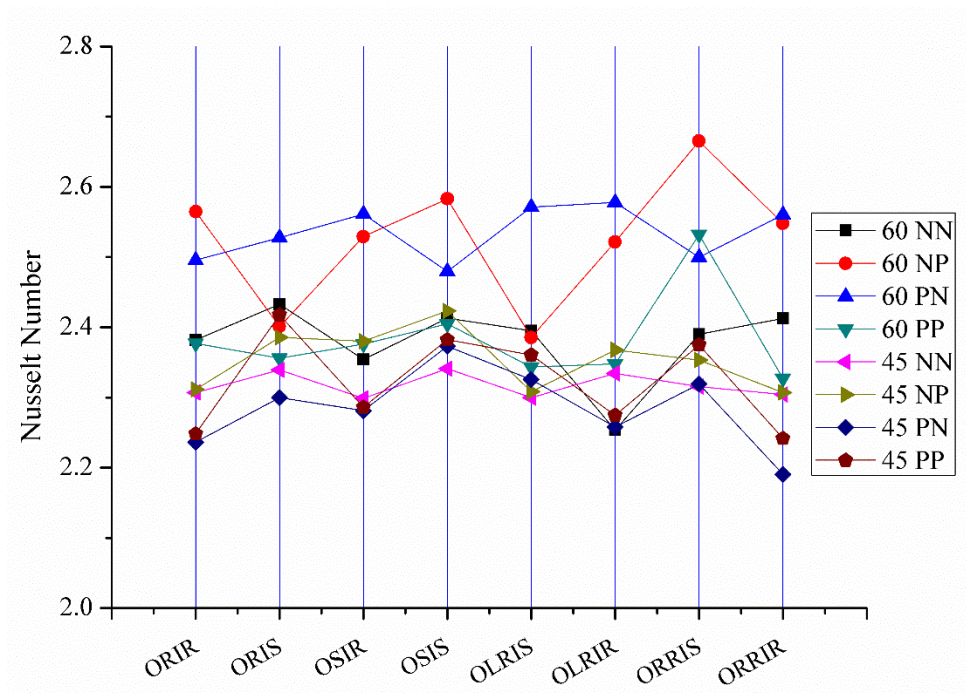


(d) 60 PP cases

Fig.4 Heat transfer and friction loss characteristics in channel with 60-degree ribs and different corner shapes



(a) Thermal performance factor for cases with 60 degree ribs



(b) Cooling performance

Fig.5 Thermal performance factor and heat transfer performance of the whole channel

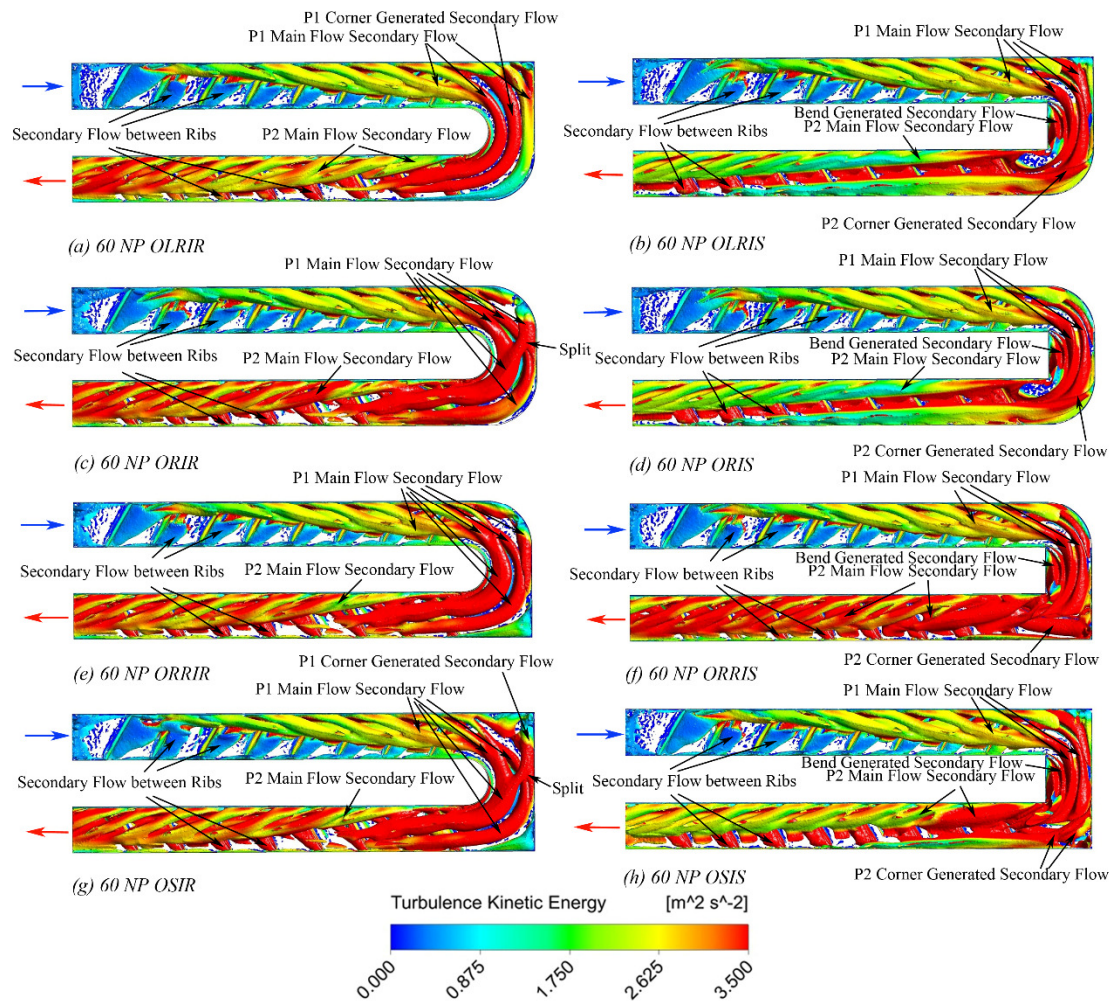
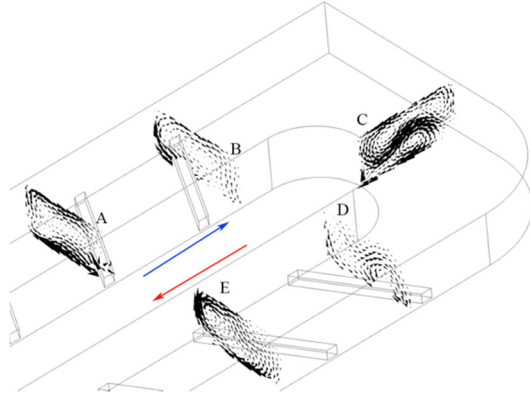
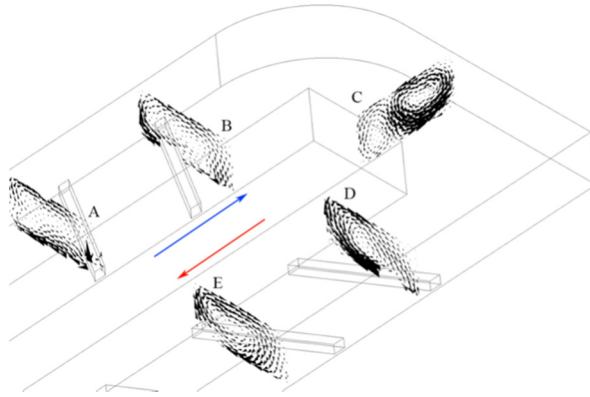


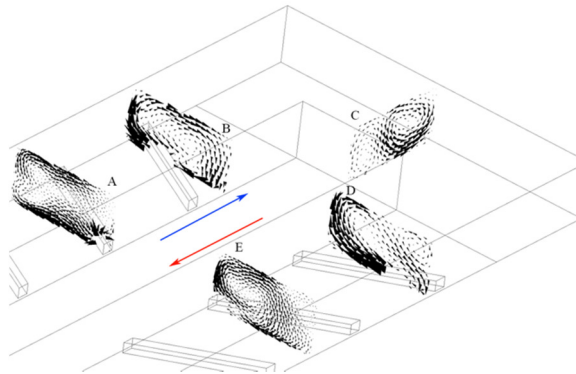
Fig.6 Secondary flow structure in 60 NP cases



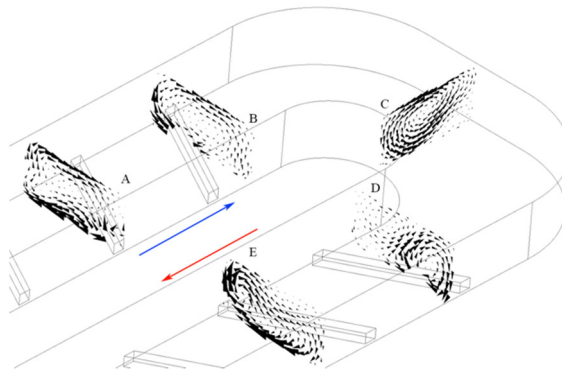
(a) 60 NP OLRIR



(b) 60 NP ORRIS



(c) 60 NP OSIS



(d) 60 NP ORIR

Fig. 7 Rotation direction of secondary flow in NP cases

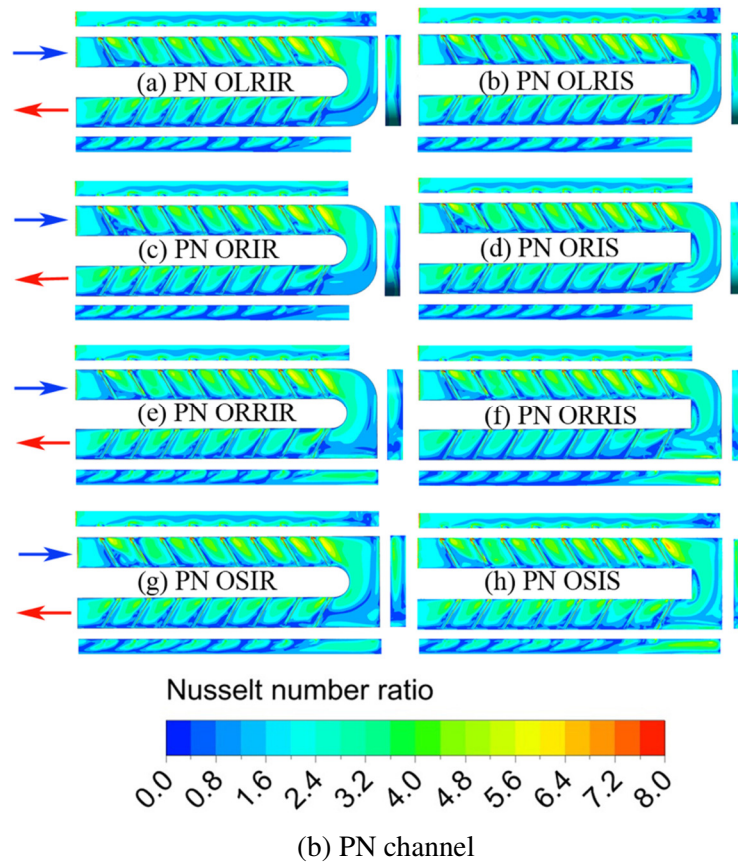
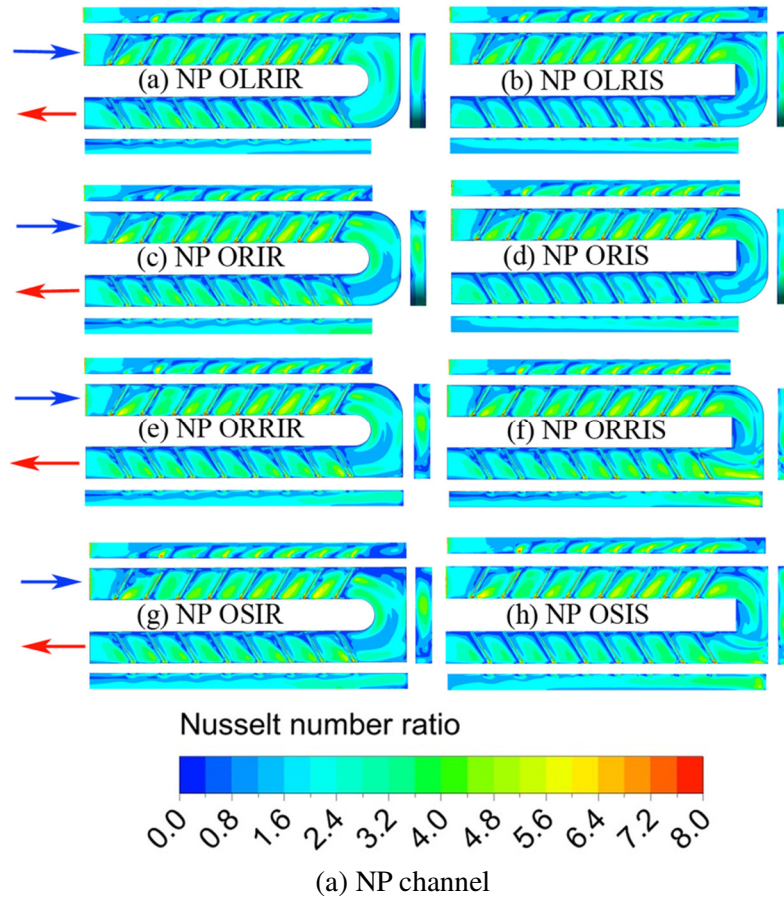


Fig.8 Nusselt number distribution contour

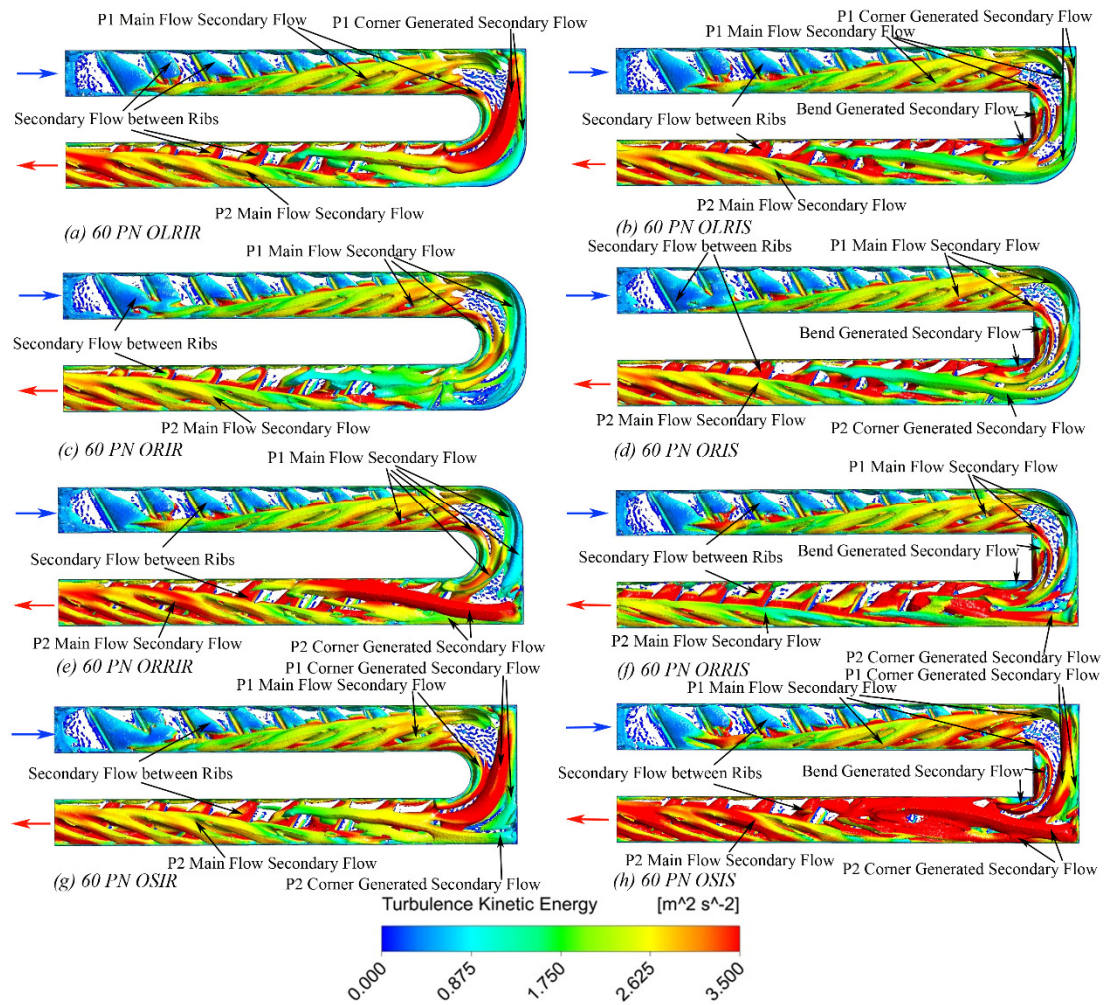
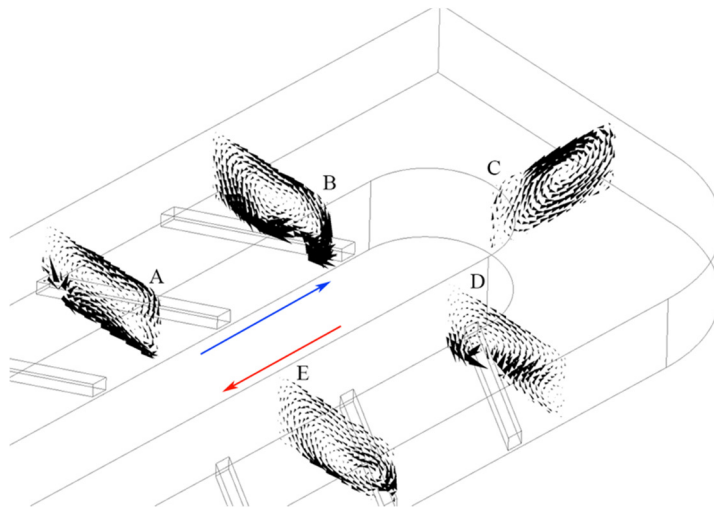
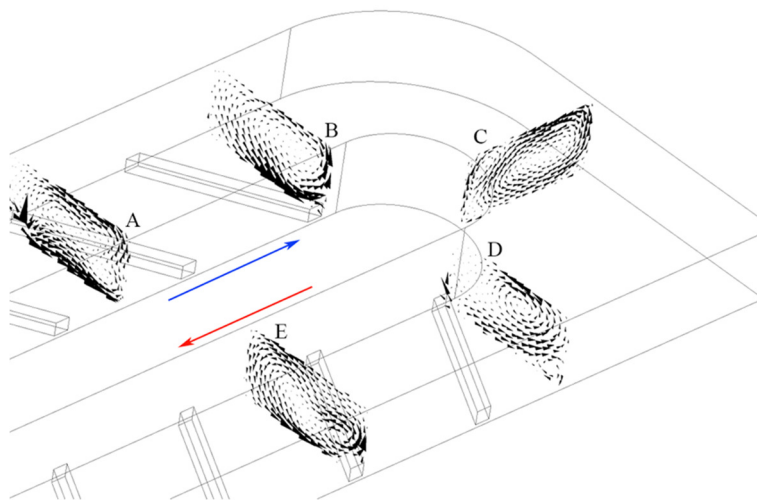


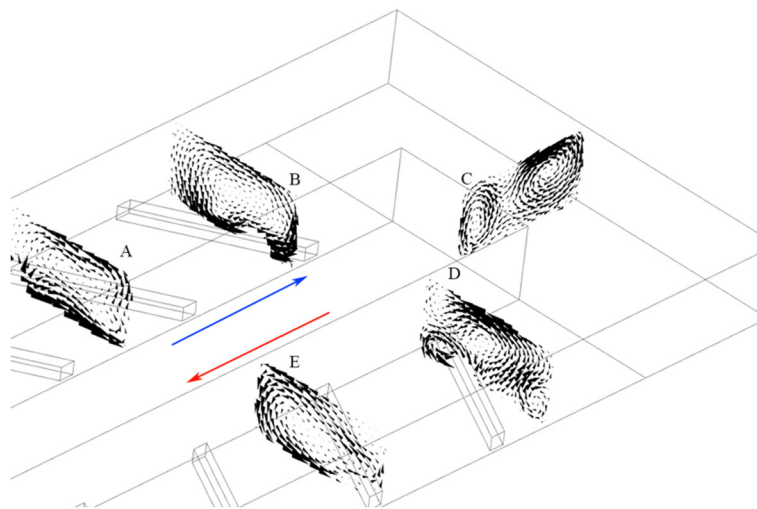
Fig.9 Secondary flow in PN cases



(a) 60 PN OLRIR



(b) 60 PN ORRIR



(c) 60 PN OSIS

Fig. 10 Rotation direction of secondary flow in PN cases